# Laboratory Modeling of Geophysical Vortices

G.J.F. van Heijst[1] and H.J.H. Clercx[1,2]

[1]JM Burgers Center and Fluid Dynamics Laboratory, Department of Physics, Eindhoven University of Technology, 5600 MB Eindhoven, The Netherlands; email: g.j.f.v.heijst@tue.nl

[2]Department of Applied Mathematics, University of Twente, 7500 AE Enschede, The Netherlands

Annu. Rev. Fluid Mech. 2009. 41:143–64

First published online as a Review in Advance on June 18, 2008

The *Annual Review of Fluid Mechanics* is online at fluid.annualreviews.org

This article's doi: 10.1146/annurev.fluid.010908.165207



0066-4189/09/0115-0143$20.00

## Key Words

rotating flow, barotropic vortices, topography, β-effect, shallow fluid layer

## Abstract

Investigators have modeled oceanic and atmospheric vortices in the laboratory in a number of different ways, employing background rotation, density effects, and geometrical confinement. In this article, we address barotropic vortices in a rotating fluid, emphasizing generation techniques, instability issues, and topography effects in particular. We then review work on vortices in shallow fluid layers, including topography effects on vortices in coastal areas and the role of vortices in tidal exchange between two connected basins.

## 1. INTRODUCTION

Vortices are abundant in large-scale geophysical flows. For example, they are observed in the form of cyclonic depression cells and tornadoes in the atmosphere and in the form of Gulf Stream rings or Agulhas rings in the oceans (e.g., see de Ruijter et al. 2004). The dynamics of geophysical vortices is primarily determined by the planetary background rotation, density stratification, and possibly confinement restrictions (their vertical scales are usually substantially smaller than their horizontal dimensions). The often complicated dynamics of these vortex structures can be studied in idealized situations in laboratory experiments, which allow the study of dynamical mechanisms in isolation. In this article we review the laboratory modeling of barotropic geophysical vortices (excluding density effects) in homogeneous rotating fluids and in shallow, homogeneous fluid layers. In addition to reviewing generation techniques and basic dynamical balances, we pay particular attention to bottom topography effects on vortex evolution.

## 2. BAROTROPIC VORTICES IN ROTATING FLUIDS

### 2.1. Theoretical Background

The relative flow in an incompressible fluid in a rotating system is described by the continuity equation and the Navier-Stokes equation

$$\nabla \cdot \mathbf{v} = 0, \tag{1}$$

$$\frac{\partial \mathbf{v}}{\partial t} + (\mathbf{v} \cdot \nabla)\mathbf{v} + 2\boldsymbol{\Omega} \times \mathbf{v} = -\frac{1}{\rho}\nabla p + \nu \nabla^2 \mathbf{v}, \tag{2}$$

where $\mathbf{v}$ is the relative velocity; $t$ is the time; $\boldsymbol{\Omega}$ is the rotation vector; $\rho$ is the density; $\nu$ is the kinematic viscosity; and $p$ is the reduced pressure, which contains gravitational and centrifugal contributions. The Coriolis term $2\boldsymbol{\Omega} \times \mathbf{v}$ describes an acceleration perpendicular to the velocity vector $\mathbf{v}$, which gives rotating flows some remarkable properties.

For large-scale geophysical flows, taking place on a rotating sphere, it is convenient to introduce a corotating Cartesian coordinate frame $(x, y, z)$, with the coordinates pointing in the local eastern, northern, and vertically upward direction, respectively, with corresponding velocity components $(u, v, w)$.

The planetary rotation vector is then decomposed as $\boldsymbol{\Omega} = (\Omega_x, \Omega_y, \Omega_z) = (0, \Omega\cos\varphi, \Omega\sin\varphi)$, where $\varphi$ is the geographical latitude. Because the large-scale motion occurs in a thin shell (i.e., with the horizontal scales much larger than the vertical ones), it is reasonable to assume that $w \ll u,\ v$. In this approach, the components of the Coriolis term become

$$2\boldsymbol{\Omega} \times \mathbf{v} = (-fv,\ fu,\ -2\Omega u\ \cos\varphi), \tag{3}$$

where $f \equiv 2\Omega\sin\varphi$ is the Coriolis parameter, expressing that the effect of the planet's rotation varies with latitude $\varphi$, being zero at the equator and reaching a maximum effect at the poles. This gradient in $f(\varphi)$ can be approximated by applying a Taylor expansion around a reference latitude $\varphi_0$. We obtain the simplest approximation by taking only the first term of the expansion, leading to $f = f_0 = 2\Omega\sin\varphi_0$. This so-called $f$-plane approximation is valid for flows with limited extent in the north-south direction. By including the next term, one obtains

$$f = f_0 + \beta y, \tag{4}$$

where $\beta = 2\Omega\cos\varphi_0/R$, with $R$ the radius of the spherical globe. This linearized version of $f(\varphi)$ is referred to as the $\beta$-plane approximation.

Typical values for moderate latitudes ($\varphi_0 = 45°$) are $f_0 \simeq 10^{-4}$ s$^{-1}$ and $\beta \simeq 2.10^{-11}$ m$^{-1}$ s$^{-1}$. Although this value of $\beta$ is rather small, for large-scale flows extending over a few thousands of kilometers in the north-south direction, the gradient in $f$ plays a crucial role.

Regardless of the type of approximation of $f$, we can write the equation of motion (Equation 2) for the horizontal flow field $\mathbf{v} = (u,\ v)$ as

$$\frac{D\mathbf{v}}{Dt} + f\,\mathbf{k} \times \mathbf{v} = -\frac{1}{\rho}\nabla p + \nu\nabla^2\mathbf{v}, \tag{5}$$

where $\mathbf{k}$ is the unit vector in the local $z$ direction, and $\frac{D}{Dt}$ represents the material derivative. Using a length scale $L$ and a velocity scale $V$, we can nondimensionalize the equation of motion (Equation 5) in the $f$-plane approximation as follows:

$$\frac{\partial\tilde{\mathbf{v}}}{\partial\tilde{t}} + Ro(\tilde{\mathbf{v}}\cdot\tilde{\nabla})\tilde{\mathbf{v}} + 2\mathbf{k}\times\tilde{\mathbf{v}} = -\tilde{\nabla}\tilde{p} + E\tilde{\nabla}^2\tilde{\mathbf{v}}, \tag{6}$$

where $Ro = \frac{V}{\frac{1}{2}fL}$ is the Rossby number and $E = \frac{\nu}{\frac{1}{2}fL^2}$ is the Ekman number, with tildes denoting dimensionless quantities and operators. (We omit the tildes from this point forward for clarity.) An interesting class of steady flows is found for $Ro \ll 1$ and $E \ll 1$, for which Equation 6 becomes

$$2\mathbf{k}\times\mathbf{v} = -\nabla p, \tag{7}$$

which represents the geostrophic balance between Coriolis and pressure-gradient forces. By taking the curl and using $\nabla\cdot\mathbf{v} = 0$, one derives from Equation 7

$$(\mathbf{k}\cdot\nabla)\mathbf{v} = 0 \rightarrow \frac{\partial\mathbf{v}}{\partial z} = 0, \tag{8}$$

which is the celebrated Taylor-Proudman theorem, stating that the flow is not dependent on the vertical coordinate $z$. Apparently, geostrophic flow is organized in the form of vertically aligned columns. G.I. Taylor experimentally verified this theorem in 1923 by slowly towing a solid obstacle along the bottom of a rotating-fluid tank. The column of stagnant fluid that was observed to be carried along with the moving obstacle is now commonly referred to as the Taylor column. Vortices generated in a homogeneous rotating fluid generally appear as axially aligned columns. Although the Taylor-Proudman theorem is formally only valid for $Ro \ll 1$ and $E \ll 1$, the tendency for columnar structures is also observed for weakly unsteady flows with $Ro = O(1)$.

Written in terms of cylindrical coordinates $(r,\ \theta)$ and velocity components $(v_r,\ v_\theta)$, the radial component of the Navier-Stokes equation for an inviscid, steady, axisymmetric vortex flow is

$$\frac{v_\theta^2}{r} + fv_\theta = \frac{1}{\rho}\frac{\partial p}{\partial r}, \tag{9}$$

where the ratio of the centrifugal acceleration term $v_\theta^2/r$ and the Coriolis term $fv_\theta$ is represented by the Rossby number. For small $Ro$ values, the term $v_\theta^2/r$ can be neglected, and the vortex is in geostrophic balance. In the case $Ro \gg 1$, the Coriolis term plays a negligible role, and the flow is in cyclostrophic balance,

$$\frac{v_\theta^2}{r} = \frac{1}{\rho}\frac{\partial p}{\partial r}, \tag{10}$$

which allows both clockwise and anticlockwise motion—in either case around a center of low pressure. For $Ro = O(1)$, the swirling flow is described by the full Equation 9 and is usually referred to as the gradient flow balance.

In addition to single, monopolar vortices, compact vortex pairs exist, which are usually referred to as dipolar vortices. Again, according to the Taylor-Proudman theorem (Equation 8), such dipolar structures manifest themselves in a rotating fluid in the form of axially aligned columns. The

horizontal cross section of these compact, coherent vorticity structures consists of two regions of opposite vorticity. The dipolar vortex hence possesses a self-propelling mechanism, and it propagates along a straight line when its structure is symmetric, whereas asymmetric dipoles move along a curved track. A solution for a symmetric, inviscid vortex dipole with vorticity confined in a circular area has been discussed by Lamb (1932) in his book *Hydrodynamics* (the second edition published in 1895, the third in 1906) and in more detail (even for asymmetric structures) by S.A. Chaplygin in 1903 (for a detailed account, see Meleshko & van Heijst 1994). More recently, investigators have developed solutions for inviscid dipolar vortex structures (modons) on a β-plane (e.g., see Flierl 1987, Khvoles et al. 2005, Kizner et al. 2003).

In a rotating fluid, vortices are commonly bounded by horizontal boundaries, which may impose a no-slip condition (at a solid boundary) or a certain shear-stress condition (e.g., owing to wind stress at the free surface of an oceanic vortex). The adjustment of the vortex flow to these boundary conditions occurs in Ekman layers, in which the viscous term in Equation 5 or 6 plays an essential role, even though $E \ll 1$. Assuming a steady vortex flow with $Ro \ll 1$, the flow outside the Ekman layers is in geostrophic balance (Equation 7). In the Ekman layers, the viscous term in Equation 6 should essentially balance the Coriolis term, implying $E\nabla^2 \sim E\frac{\partial^2}{\partial z^2} \sim O(1)$. Apparently, the nondimensional Ekman layer thickness is $\tilde{\delta}_E \sim E^{1/2}$, and in dimensional form,

$$\delta_E = L\tilde{\delta}_E = LE^{1/2} = \left(\frac{2\nu}{f}\right)^{1/2}. \tag{11}$$

In a typical rotating-tank experiment with water as the working medium ($\nu = 10^{-6}$ m$^2$ s$^{-1}$), rotation speed $\frac{1}{2}f = \Omega = 1$ s$^{-1}$, and a typical length scale $L \simeq 0.3$ m, the Ekman number has a value $E \simeq 10^{-5}$, and the Ekman layer thickness is $\delta_E \simeq 1$ mm. Although very thin compared to the fluid depth, the viscous layer plays an essential role, as discussed below. We note that the Ekman layer thickness $\delta_E = (\nu/\Omega)^{1/2}$ is independent of the length scale $L$ of the flow structure or the size of the domain.

Choosing the (nondimensional) horizontal velocities in the Ekman layer to be $O(1)$ (i.e., of the same order of magnitude as the geostrophic interior flow), the (nondimensional) radial volume transport in the Ekman layer is $O(E^{1/2})$. Depending on the structure of the geostrophic interior flow outside the Ekman layer, horizontal divergence/convergence in the layer implies vertical velocities of $O(E^{1/2})$ in the form of suction or blowing. This is expressed in the so-called suction condition, which, for the case of a geostrophic flow above a no-slip bottom at $z = 0$, reads

$$w_E(z = \delta_E) = \frac{1}{2}\delta_E\omega_I, \tag{12}$$

where $\omega_I$ is the vorticity of the geostrophic interior flow. For example, for a cyclonic vortex ($\omega_I > 0$), a radially inward flow is present in the Ekman layer, resulting in blowing ($w_E > 0$). In this way the Ekman layer is active in setting up a weak $O(E^{1/2})$ circulation in the geostrophic flow region, which results in the spin-down or spin-up of that interior flow. This adjustment process takes place on the Ekman timescale $T_E = H/(\nu\Omega)^{1/2}$, where $H$ is the fluid depth above the Ekman layer.

Because of the columnar structure of rotating flows with $Ro \lesssim O(1)$, we may consider the flow as quasi–two dimensional (i.e., with vertical velocities much smaller than the horizontal velocities). In other words, the vorticity vector of the relative flow points in the local vertical direction: $\boldsymbol{\omega} = \omega\mathbf{k}$. By taking the curl of Equation 5, we derive the vorticity equation

$$\frac{\partial\omega}{\partial t} + u\frac{\partial\omega}{\partial x} + v\frac{\partial\omega}{\partial y} + \left(\frac{\partial u}{\partial x} + \frac{\partial v}{\partial y}\right)(\omega + f) = \nu\nabla^2\omega, \tag{13}$$

where $\omega = \frac{\partial v}{\partial x} - \frac{\partial u}{\partial y}$.

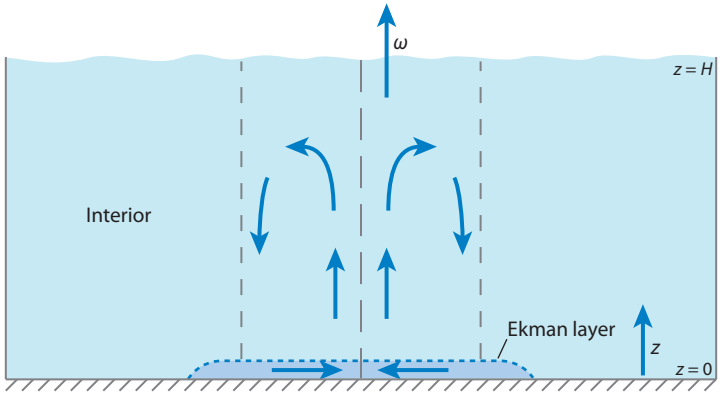


**Figure 1**

Schematic drawing of the secondary circulation in a cyclonic vortex driven by the Ekman layer at the tank bottom.

Integration of the continuity equation over the fluid depth $H$ yields

$$\left(\frac{\partial u}{\partial x}+\frac{\partial v}{\partial y}\right)=-\left[w(z=H)-w(z=0)\right]/H. \tag{14}$$

It is now assumed that the fluid is bounded by a solid flat bottom at $z = 0$ and a flat nonmoving free surface at $z = H$, so that $w(z = H) = 0$, and $w(z = 0)$ is given by the Ekman suction condition (Equation 12). After substituting this into Equation 13, the vorticity equation becomes

$$\frac{\partial \omega}{\partial t}+u\frac{\partial \omega}{\partial x}+v\frac{\partial \omega}{\partial y}=\nu\nabla^2\omega-\frac{1}{2}E^{1/2}\omega(\omega+f). \tag{15}$$

When the Rossby number ($Ro \sim |\omega|/f$) is small, the nonlinear Ekman term is usually replaced by its linear version $-\frac{1}{2}E^{1/2}f\omega$. However, for moderate $Ro$ values (as encountered in many geophysical and laboratory situations), one should keep the nonlinear term. A remarkable feature of this nonlinear condition is the symmetry breaking associated with the term $\omega(\omega+f)$: It appears that cyclonic vortices ($\omega > 0$) show a faster decay than anticyclonic vortices ($\omega < 0$) with the same $Ro$ value.

We can further refine the vorticity equation (Equation 15) by including the weak $O(E^{1/2})$ circulation driven by the bottom Ekman layer (**Figure 1**). This results in

$$\frac{\partial \omega}{\partial t}+\mathcal{J}(\omega,\ \Psi)-\frac{1}{2}E^{1/2}\nabla\Psi\cdot\nabla\omega=\nu\nabla^2\omega-\frac{1}{2}E^{1/2}\omega(\omega+f), \tag{16}$$

where $\mathcal{J}$ is the Jacobian operator, and $\Psi$ is the stream function, defined as $\mathbf{v} = \nabla \times (\Psi\mathbf{k})$ (see Zavala Sansón & van Heijst 2002). Although the additional terms are $O(E^{1/2})$ and therefore small, they may have an important effect on the evolution of the interior flow, as discussed below.

In the shallow-layer approximation (i.e., under the assumption of quasi-geostrophic column-like motion in a layer of inviscid fluid), the potential vorticity $Q = (f + \omega)/H$ is conserved (see Pedlosky 1987):

$$\frac{D}{Dt}\left(\frac{f+\omega}{H}\right)=0. \tag{17}$$

The gradient in the planetary vorticity $f$ leads to remarkable behavior, as can be appreciated when considering a vortex in a fluid layer with a constant depth $H_0$. When shifted northward into regions of larger $f$ values, the relative vorticity $\omega$ should decrease to keep the potential vorticity

$Q$ constant. Apparently, a cyclonic vortex ($\omega_0 > 0$) moving northward becomes weaker, whereas an anticyclonic vortex ($\omega_0 < 0$) intensifies when shifted to the north.

Conservation of the potential vorticity $Q$, as expressed by Equation 17, can now be exploited to model the planetary β-effect in a rotating fluid by applying a suitably chosen bottom topography. As reviewed by van Heijst (1994), for shallow topography (height variations $\Delta h \ll H$) and small $Ro$ values, we can model the planetary β-effect implied by $f = f_0 + \beta y$ by a linearly sloping bottom so that $H(y) = H_0(1 - \alpha y)$. This is commonly referred to as the topographic β-plane. Fluid parcels moving into shallower parts in a rotating-fluid tank experience a dynamically similar effect when moving northward on a rotating globe: Their relative vorticity $\omega$ decreases. Similar to the asymmetry observed for the geophysical case, a cyclonic vortex ($\omega_0 > 0$) climbing the topography becomes weaker, whereas an anticyclonic vortex ($\omega_0 < 0$) moving into shallow water is intensified.

## 2.2. Vortex Generation Techniques

Vortices can be generated in a rotating fluid in a number of different ways, usually leading to vortex structures with somewhat different characteristics. One generation method for monopolar vortices is the sink technique, by which a cyclonic vortex is produced by pumping out some fluid through a sink, either located in one point or distributed along a line. By sucking the fluid away through a perforated tube positioned vertically in the rotating fluid (see **Figure 2*a***), fluid parcels are deflected to the right when moving toward the sink (as implied by conservation of angular momentum or, alternatively, the action of the Coriolis acceleration), until eventually an approximate gradient flow balance (Equation 9) is reached. At this stage, the vortex motion takes on the appearance of a vertically aligned columnar vortex, even though the Rossby number may be $Ro > 1$. Kloosterziel & van Heijst (1992) have applied this technique, and they found that after stopping the forcing by vertically lifting the tube out of the fluid, the barotropic, cyclonic vortices thus generated have a vorticity and velocity profile that are well approximated by the following expressions:

$$\omega(r) = \omega_0 \exp\left(-\frac{r^2}{R^2}\right), \tag{18a}$$

$$v_\theta(r) = \frac{\omega_0 R^2}{2r}\left[1 - \exp\left(-\frac{r^2}{R^2}\right)\right], \tag{18b}$$

where $\omega_0$ is the peak vorticity, $R$ is a horizontal length scale, and $r$ is the radial distance to the vortex axis. The circulation of such vortices has a nonzero value. Many authors have applied

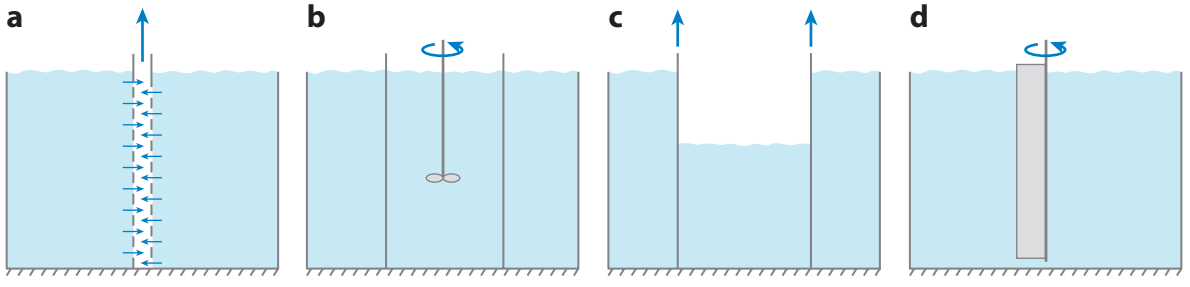


**Figure 2**

Generation techniques of barotropic vortices in a rotating fluid: (*a*) sucking fluid away through a perforated tube, (*b*) stirring fluid in a thin-walled open cylinder, (*c*) gravitational collapse, and (*d*) rotating or moving a flap through the rotating fluid. In all cases, after the forcing, the devices are removed by vertically lifting them out of the fluid.

this sink or suction technique (Flór & Eames 2002; Trieling et al. 1998; Zavala Sansón & van Heijst 2002; R.R. Trieling, R.P.J. Kunnen & G.J.F. van Heijst, manuscript submitted). The Ekman layer at the tank bottom plays an important role in the spin-down (or spin-up) of vortices. Kloosterziel & van Heijst (1992) studied the decay of barotropic vortices in a rotating fluid in detail and analyzed the observed spin-down process. Maas (1993) extended this analysis by including nonlinear and surface deformation effects.

The stirring technique produces a different type of barotropic vortex: Fluid confined in a thin-walled, bottomless vertical cylinder inserted into the rotating fluid is stirred (see **Figure 2*b***) and then left to develop into an axisymmetric vertical flow. By vertically lifting this confining cylinder, one releases the vortex in the ambient rotating fluid. Kloosterziel & van Heijst (1991) found experimentally that the swirling motion of such cyclonic vortices soon after release is well approximated by the following profiles for the vorticity and the azimuthal velocity:

$$\omega(r) = \omega_0 \left(1 - \frac{1}{2}\alpha \left(\frac{r}{R}\right)^{\alpha}\right) \exp\left(-\left(\frac{r}{R}\right)^{\alpha}\right), \tag{19a}$$

$$v_\theta(r) = \frac{1}{2}\omega_0 r \exp\left(-\left(\frac{r}{R}\right)^{\alpha}\right), \tag{19b}$$

where $\alpha$ is a parameter controlling the shape of the profiles. In most experiments, one finds $\alpha$ values close to 2. The vortices thus produced are essentially isolated, in the sense that their total circulation is zero because the initial swirling fluid body was confined in a cylinder with a no-slip inner wall. In other words, the vortex core is surrounded by a shell of oppositely signed vorticity. This vorticity structure may possibly lead to instability of the vortex. In contrast to their cyclonic counterparts, anticyclonic vortices produced by the stirring technique are highly unstable, revealing strong three-dimensional overturning motion immediately after release (Kloosterziel & van Heijst 1991). The stirring technique has been used to produce cyclonic vortices—in particular, in experiments on the effects of bottom topography (e.g., Flór & Eames 2002, Velasco Fuentes et al. 1996, Voropayev et al. 1999, Zavala Sansón & van Heijst 2002).

Kloosterziel & van Heijst (1992) applied a third method, the so-called gravitational collapse technique, to create cyclonic vortices. For this purpose, a thin-walled open cylinder is placed concentrically in the rotating-fluid tank, with the fluid level inside this cylinder lower than that outside (see **Figure 2*c***). When the cylinder is lifted, a gravity-driven flow arises in the radial direction, immediately followed by a deflection due to the Coriolis acceleration. After a short period, an equilibrium state is reached in which the motion is close to purely azimuthal. Velocity measurements have revealed that, for the case of stable vortices, the collapse vortices tend to evolve toward the same vorticity and velocity distributions (Equation 19) as measured for the stirring vortices (Kloosterziel & van Heijst 1992). J.B. Flór (private communication) used a related generation method by vertically lifting a partially tapered solid cylinder inserted into the rotating fluid prior to the start of the experiment. The volume initially occupied by the solid cylinder is immediately filled with fluid, which acquires a cyclonic swirling velocity component when flowing radially to this region, similar to collapse-produced vortices.

In an alternative way, Afanasyev (2002) has produced barotropic vortices—both cyclonic and anticyclonic—by rotating a solid flap over a certain angle (see **Figure 2*d***). One disadvantage of this technique is that, in addition to the (almost-circular) starting vortex, a (deformed) stopping vortex is generated. The anticyclonic part of this vortex pair was mostly observed to be unstable, showing centrifugal instability features as in Kloosterziel & van Heijst's (1991) earlier experiments.

Dipolar vortex structures have been created in a rotating fluid by locally introducing linear momentum in the fluid in the form of a pulsed jet flow through a vertical slit (see Kloosterziel et al. 1993, Carnevale & Kloosterziel 1994b). To avoid deflection of the jet by Coriolis forces, as

encountered in the experiment by Flierl et al. (1983), a flat plate was mounted on the right-hand side of the split looking downstream. In this way, a more or less symmetric dipole could be generated, moving along a straight track.

In their experiments on dipolar vortices over a topographic β-plane, Velasco Fuentes & van Heijst (1994) applied a different generation technique, namely a slowly moving open cylinder that is gradually lifted out of the rotating fluid. When the cylinder is moved slowly along a straight line, a symmetric wake arises—depending on the speed of translation. After the cylinder is withdrawn vertically, this wake flow becomes organized in a symmetric, columnar dipole structure. In the absence of topography effects, the symmetric dipoles thus generated are Lamb-Chaplygin-like, with the vorticity concentrated in a circular cross-sectional area and with a linear relationship between the relative vorticity $\omega$ and the stream function $\Psi$. Zavala Sansón et al. (2001) applied this same technique in their experimental study of decaying dipolar vortices due to nonlinear Ekman effects, as described by Equation 16.

Recently, Trieling et al. (R.R. Trieling, R. Santbergen, G.J.F. van Heijst & Z. Kizner, manuscript submitted) performed experiments on vortex dipoles with noncircular cross sections. Such vortices, whose properties were studied theoretically by Kizner et al. (2003) and Khvoles et al. (2005), are generated by slowly moving a vertical plate horizontally through the fluid, in a direction perpendicular to its plane. After the plate is gradually lifted out of the fluid, the vortices arising from flow separation at both plate edges combine in a dipolar structure—depending on the width $W$ of the plate. With a proper choice of the experimental parameters (width $W$, speed, and path length of the plate), dipolar vortex structures could be created with vorticity contained in an elliptical cross-sectional area.

## 2.3. Instability

Columnar vortices in a rotating fluid may become unstable through different mechanisms, such as barotropic or shear instability, which has a purely two-dimensional character. Generally, a barotropic instability may occur when the vorticity changes sign at some radius measured from the vortex axis. Vortices with single-signed vorticity (such as the vortices produced by the sink method) are stable according to this Rayleigh inflection-point theorem, as well as nonlinear stability analyses (e.g., see Carnevale & Shepherd 1990, Drazin & Reid 1981). Isolated vortices (such as those produced by the stirring method) do not have a single-signed vorticity structure and hence are susceptible to barotropic instability. Van Heijst & Kloosterziel (1989; Kloosterziel & van Heijst 1991) first studied this type of instability experimentally. One striking manifestation of a barotropic instability is the growth of a wave number $m = 2$ perturbation, leading to the formation of a tripolar vortex. Even a higher–wave number instability ($m = 3$) was found in rotating-fluid experiments by Carnevale & Kloosterziel (1994a) and Beckers & van Heijst (1998). The mechanism of the shear instability has been studied theoretically and numerically as well (e.g., see Carnevale & Kloosterziel 1994a, Kloosterziel & Carnevale 1999, Orlandi & Carnevale 1999). Columnar vortices in a rotating fluid may also become centrifugally unstable, with perturbations leading to essentially three-dimensional overturning motions. Kloosterziel & van Heijst (1991) observed experimentally this type of instability, which led to their extension of Rayleigh's criterion for centrifugal instability. For vortex flow on an $f$ plane, the extended Rayleigh instability criterion is

$$\frac{d}{dr}\left(rv_\theta + \frac{1}{2}fr^2\right)^2 < 0. \tag{20}$$

This extended criterion applies also to (either centered or off-center) vortices in a rotating fluid, with $f = 2\Omega$, and reads $(v_\theta + \Omega r)(\omega + 2\Omega) < 0$, implying stability if $v_{abs} \cdot \omega_{abs} > 0$ at all positions in the

vortex flow. Kloosterziel & van Heijst (1991) have examined the possible centrifugal instability of isolated (stirring-induced vortices) in detail. Although the behavior is essentially dependent on the Rossby radius $Ro$, generally only very weak anticyclonic vortices are centrifugally stable, whereas only very strong cyclonic vortices are centrifugally unstable. Afanasyev & Peltier (1998) observed this behavior experimentally, generating a swirling flow in a rotating fluid locally using a rotating solid cylinder immersed in the fluid.

Centrifugal instability of barotropic vortices in a rotating fluid also has been investigated in a number of theoretical/numerical studies (e.g., see Billant & Gallaire 2005, Carnevale et al. 1997, Gallaire & Chomaz 2003, Orlandi & Carnevale 1999, Sipp & Jacquin 2000). These studies have contributed to our understanding of the instability mechanisms and have led to further generalizations of the instability criterion.

## 2.4. Topography Effects

Because topography effects play an important role in planetary flows, we highlight some experimental studies on vortex structures over bottom topography, distinguishing between monopolar and dipolar vortices.

**2.4.1. Monopolar vortices.** Single, monopolar vortices have been studied, both experimentally and numerically, for different topographic configurations, including uniformly sloping bottom (topographic β-plane), step, coastal topography, and ridge.

***2.4.1.1. Topographic β-plane.*** Whereas a monopolar vortex released on an $f$ plane shows no drift, the β-plane provides a propagation mechanism, which can be understood from conservation of potential vorticity $(f + \omega)/H$, as expressed by Equation 17. For example, when moving northward/southward, fluid parcels in a vortex acquire additional negative/positive relative vorticity, leading to the formation of so-called β-gyres, which can be considered as a dipolar vorticity anomaly on top of the primary monopolar vortex. As a result, the vortex initially shows a slow drift northward. In the case of a cyclonic vortex, the axis of this dipolar perturbation vorticity field is rotated in the cyclonic direction. The whole structure is then carried toward the northwest owing to the self-induced drift of this dipolar perturbation. Similarly, anticyclonic vortices show an initial drift to the southwest. This β-induced drift behavior of monopolar vortices was first analyzed by Rossby (1948) and Adem (1956), followed by a large number of studies since. The initial drift behavior has been demonstrated experimentally (e.g., Carnevale et al. 1991) and numerically (e.g., Sutyrin et al. 1994). The vortex trajectories are crucially dependent on the initial distribution and strength of the vorticity. In Carnevale et al.'s (1991) laboratory experiments, they generated cyclonic monopolar vortices on a topographic β-plane by using both the stirring method and the sink method, leading to vorticity profiles (Equation 19a), with $\alpha = 2$, and Equation 18a, respectively. Whereas the sink-induced vortices show a regular, more or less constant drift in the northwestern direction, the stirring-induced vortices follow a less smooth path. The latter vortex is isolated (i.e., its total circulation is zero): The core of positive vorticity is surrounded by a ring of negative vorticity. Dye-visualization experiments by Carnevale and colleagues (1991; Carnevale & Kloosterziel 1994b) have revealed that this outer vorticity ring is quickly deformed, and lobes are shed during the vortex drift. The vortex thus leaks vorticity, whereas its core remains rather coherent. This behavior is in contrast with that of the sink-induced vortex: This single-signed vorticity structure did not show any shedding of vorticity lobes. Flór & Eames (2002) carried out more detailed experiments on isolated and nonisolated vortices on a β-plane. While the vortex structure moves over the (topographic) β-plane, it also sets up (topographic) Rossby waves. In this

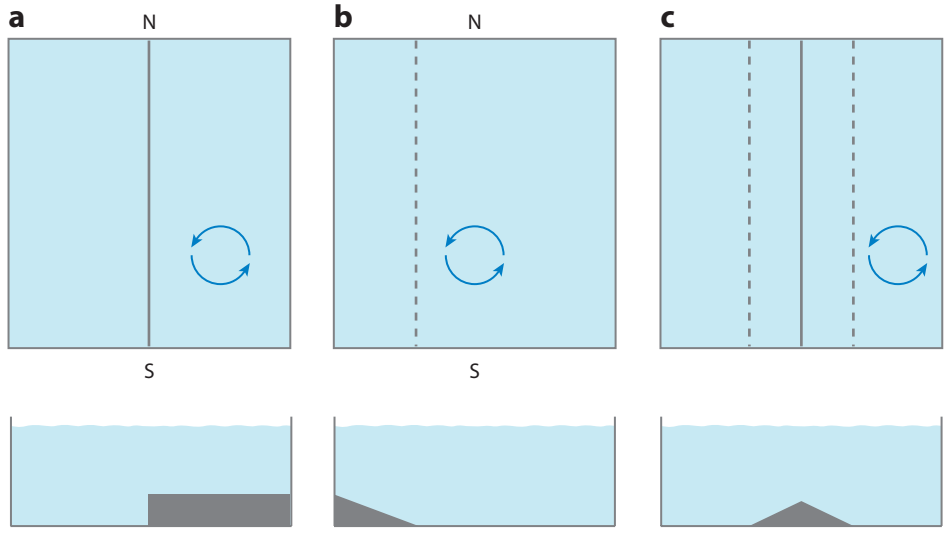


**Figure 3**

Schematic drawings of the (*a*) step, (*b*) coastal, and (*c*) ridge topography. Whereas the ridge topography is mounted on a flat bottom, the step and coastal topographies are mounted on an overall topographic β-plane. The circles indicate the initial vortex positions. The symbols N and S represent the compass directions north and south on the overall topographic β-plane, corresponding with shallow and deeper domain parts, respectively.

way, kinetic energy is drained form the vortex, leading to a decrease of its strength and a slower drift speed. Investigators have addressed this complicated evolution of the vortex in the later stages (e.g., Llewellyn Smith 1997, McDonald 1998, Reznik et al. 2000).

***2.4.1.2. Step-shaped topography.*** Zavala Sansón et al. (1999a) performed an experimental/numerical study of barotropic vortices approaching step-like bottom topography. For this purpose, they used an overall topographic β-plane on which sink-generated vortices traveled in the northwest direction and were thus forced to approach the step (see **Figure 3*a***).

The initial vortex is characterized by its peak vorticity $\omega_0$, and it moves in fluid of depth $H_0$ toward the step. On the other side of the step, the fluid depth is $H_0 + \Delta H$. In this notation, $\Delta H > 0$ and $\Delta H < 0$ denote step-down and step-up topographies, respectively. The vortices in the $\omega_0 \Delta H > 0$ case (i.e., cyclonic vortex approaching a downward step or anticyclonic vortex approaching an upward step) behave differently from those in the $\omega_0 \Delta H < 0$ case: In the latter case, the vortex usually crosses the step without any major distortions, whereas in the former case, the vortex appears to be unable to cross the step, and even appears to be reflected. This behavior can be explained by the generation of relative vorticity associated with the advection of fluid across the step. A detailed discussion is given by Zavala Sansón et al. (1999a). These authors have also studied the case of anticyclonic vortices approaching upward and downward steps using numerical flow simulations, because of the experimental difficulty of producing stable anticyclonic vortices in the rotating fluid, as discussed in Section 2.3 (see also Kloosterziel & van Heijst 1991). In the shallow-water approximation, vertical integration of the continuity equation yields $\partial(hu)/\partial x + \partial(hv)/\partial y = 0$, where $h(x, y)$ is the local fluid depth, and $(u, v)$ are the velocity components in the $(x, y)$ directions. Thus, we can define a stream function $\psi$ as $hu = \frac{\partial \psi}{\partial y}$, $hv = -\frac{\partial \psi}{\partial x}$. Disregarding Ekman suction effects, the evolution of

the relative vorticity $\omega$ is then governed by

$$\frac{\partial \omega}{\partial t} + \mathcal{J}\left(\frac{\omega + f_0 + \beta y}{h}, \psi\right) = \nu \nabla^2 \omega. \tag{21}$$

From the definitions of $\omega$ and $\psi$, it is verified that

$$\omega = -\nabla \cdot \left(\frac{1}{h}\nabla\psi\right) = -\frac{1}{h}\nabla^2\psi + \frac{1}{h^2}\nabla h \cdot \nabla\psi. \tag{22}$$

Initialized with the vorticity profile (Equation 18a) for a sink-induced vortex, the simulations based on this relatively simply barotropic model showed good agreement with experiments, at least for times smaller than the Ekman decay time $T_E$. Dunn et al. (2001) have analyzed the behavior of vortices near step-like topography by applying the methods of contour dynamics and arrived at similar results.

Zavala Sansón & van Heijst (2000) have investigated the behavior of barotropic vortices over linear, coastal bottom topography through laboratory experiments and numerical simulations. In a rotating tank, they used an overall topographic β-plane to simulate the gradient in the Coriolis parameter and hence to promote a northwestward drift of cyclonic vortices. At the western boundary of the domain, an additional sloping bottom was mounted (**Figure 3*b***). A cyclonic vortex, generated by the sink method at some distance from the western wall, initially travels in the northwestern direction until it reaches the strong coastal topography. Above this sloping bottom at the coast, it starts to climb the topography according to the local northwest rule (i.e., in the overall southwestern direction) until it is dissipated. This is clearly observed in the dye visualizations shown in **Figure 4*a***. As soon as the vortex climbs the coastal slope, a growing lobe develops in the northwest part of the vortex, which subsequently moves gradually to the north in a meandering fashion. In addition, in connection with the meanders, new cyclonic vortices are formed. These are not visible in **Figure 4*a***, as they are formed in the undyed ambient fluid. Numerical simulations, based on the same barotropic model (Equation 21) discussed above, have revealed the detailed structure of the flow over the coastal slope. **Figure 4*b*** presents numerically calculated vorticity distributions corresponding to the experimental dye photographs in **Figure 4*a***, revealing the newly formed cyclonic vortices in the northward meandering current. Of course, the flow features change slightly when the slope of the coastal topography is changed, although the gross features are preserved. As in previous cases mentioned above, the anticyclonic vortex behaves completely differently: As the vortex moves to the southwest, fluid over the slope is displaced downhill, north of the anticyclone. Owing to stretching effects, this fluid acquires positive relative vorticity, which combines with the primary vortex to form a dipolar structure. This pair then moves eastward, away from the coastal topography. Apparently, the anticyclonic vortex cannot climb the coastal slope but is instead reflected.

This behavior is in remarkable contrast to that observed when a vortex (either cyclonic or anticyclonic) arrives at a vertical western wall without coastal slope (see also Zavala Sansón et al. 1999b). In that case, the vortex remains almost at a fixed latitude, just slowly drifting southward, while leaking fluid and hence decaying.

***2.4.1.3. Ridge on an f plane.*** Zavala Sansón (2002) studied the behavior of a barotropic vortex near a topographic ridge on an *f* plane (see **Figure 3*c***) through laboratory experiments in a rotating tank and numerical simulations. The behavior of oceanic vortices near bottom ridges has also been addressed in numerical studies (e.g., van Geffen & Davies 1999, 2000), whereas Zehnder (1993) and Zehnder & Reeder (1997) concentrated on the case of an atmospheric cyclone in the presence of an idealized range of mountains.

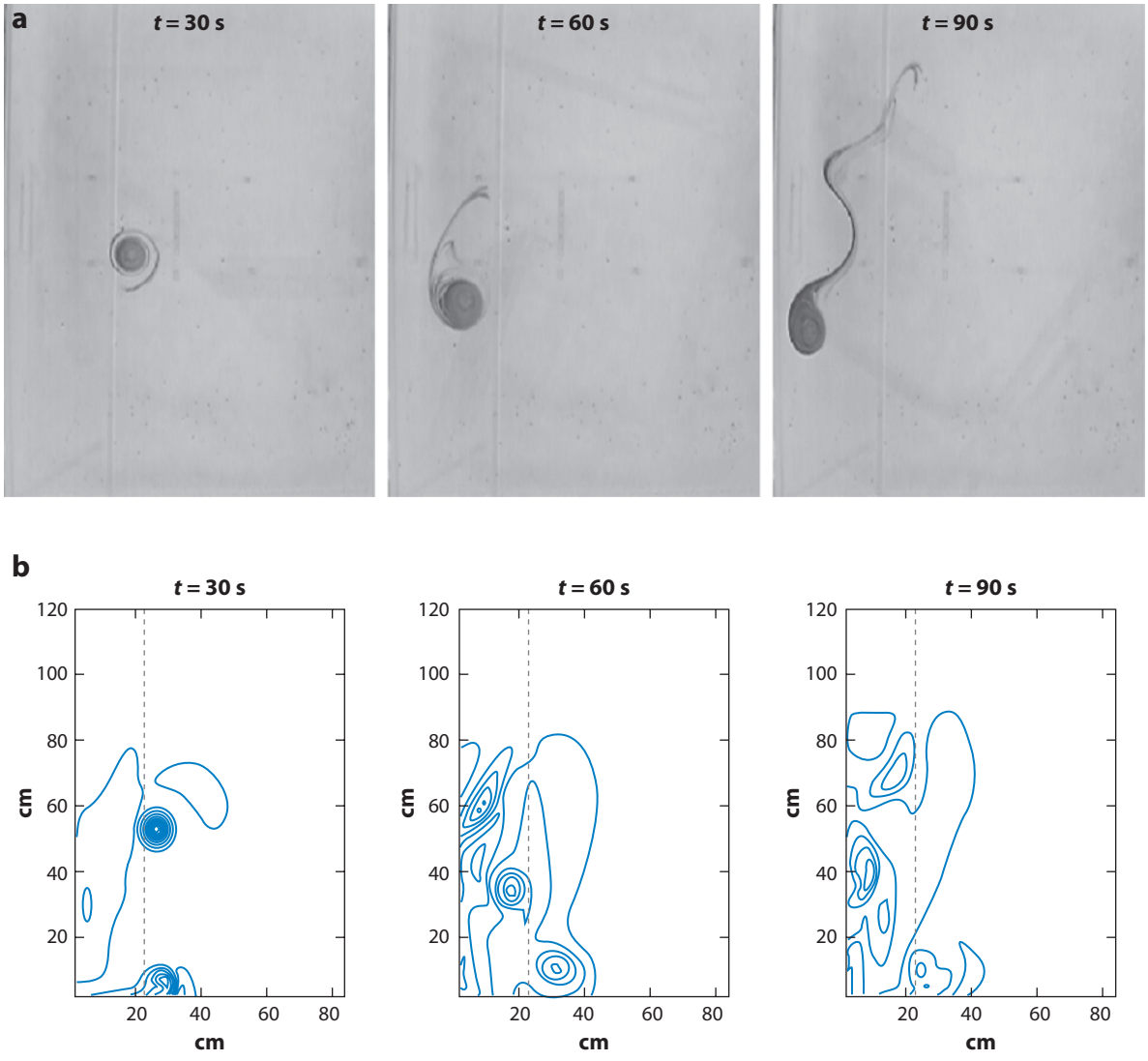


**Figure 4**

(*a*) Dye visualization of the cyclonic vortex over the coastal topography. (*b*) Numerically calculated streamline plots. Figure taken from Zavala Sansón & van Heijst 2000.

**2.4.2. Dipolar vortices.** In the absence of any background flow, the symmetric vortex dipole travels on an $f$ plane steady along a straight track, whereas the asymmetric dipole moves steadily along a circular path. On a β-plane, however, the gradient of the background vorticity leads to more complicated behavior, as may be understood from conservation of potential vorticity $(f + \omega)/H$: Any northward/southward motion leads to changes in the relative vorticity $\omega$. As discussed in Section 2.1, a northward-moving cyclonic vortex becomes weaker, whereas a northward-moving anticyclonic vortex is intensified. This implies that a vortex dipole initially traveling in a direction at a certain angle $\alpha_0$ with respect to the west-east axis becomes asymmetric: Its cyclonic part becomes weaker, whereas its anticyclonic part intensifies. This asymmetric dipole moves along a

curved path back to its initial latitude, at which its symmetry is restored. The dipole now moves under an angle $-\alpha_0$ with respect to the west-east axis, overshoots, and becomes asymmetric again. Now the cyclonic part is more intense and the anticyclonic part is weaker, so it bends back to its original latitude. This cycle is repeated, and the vortex dipole travels in a meandering way toward the east. For larger initial angles $\alpha_0$, the dipole may show a cycloid-like motion in the western direction (see McWilliams & Zabusky 1982, Velasco Fuentes & van Heijst 1994).

In reality, the dipole's behavior is more complicated than that described above, and it is governed by the full barotropic vorticity equation including the β-effect, as formulated by Equation 21. This equation does include the β-effect and topography effects, although it does not contain terms describing Ekman suction as in Equation 16. A general theoretical description of the dipole flow evolution on a β-plane is not available, but a number of numerical simulations have added to our understanding (e.g., see Sutyrin et al. 1994).

Laboratory experiments by Kloosterziel et al. (1993) and Velasco Fuentes & van Heijst (1994) have confirmed the meandering motion of the dipolar vortex on a topographic β-plane when it moves in a direction nonparallel to the topographic contours. In these experiments, the authors generated the dipoles by injection through a vertical slit and by a moving cylinder, respectively, as described in Section 2.2.

Quite a few studies have been devoted to the interaction of vortices on the β-plane, in particular to collisions of dipolar structures (e.g., see Hobson 1992, Kono & Yamagata 1977, McWilliams & Zabusky 1982). Velasco Fuentes & van Heijst (1995) studied head-on collisions experimentally and numerically. During the collision, partner exchange took place, leading to two new dipoles: one moving northward and the other moving southward. Owing to the β-effect, these dipoles became asymmetric and traveled along loop-shaped tracks toward the east.

Tenreiro et al. (2006) investigated the behavior of a barotropic dipolar vortex near a step-shaped bottom topography on an *f* plane experimentally and numerically. They examined two different step heights $\Delta h$: a low step, with $\Delta h/H_0 = 0.05$, and a high step, with $\Delta h/H_0 = 0.25$, where $H_0$ is the fluid depth on the deep side of the step. In both cases, the value of the Rossby number based on the vortex dipole was smaller than 1. The dipoles approaching the step, either from the deep or from the shallow part, behave differently in both cases. For the low-step case, the dipole is able to cross the step, after which it moves along a deflected trajectory: When crossing a step up (step down), the deflection is to the right (left) [i.e., in anticyclonic (cyclonic) direction]. As on the (topographic) β-plane, this deflection can be explained by the conservation of potential vorticity, leading to an asymmetric dipolar structure. Another feature observed in Tenreiro et al.'s (2006) experiments, and confirmed by their simulations with the barotropic model (Equation 21) extended with Ekman suction as formulated in Equation 16, is the occurrence of a weak current along the step, with the shallower side on its right. The origin of this current is directly associated with ambient fluid being pushed back over the step when the dipole crosses it.

In contrast, in the high-step case, the dipole is not able to cross the step and instead splits into two parts. When the dipole approaches the step from the deeper side, its anticyclonic part is reflected when it pairs with a patch of cyclonic vorticity, generated as fluid is pushed back from shallow to deep water. This reflection mechanism is similar to what Zavala Sansón et al. (1999a) observed for the monopolar vortex reflection near a step. The other part of the original dipole is deformed and drifts along the step, with the shallower part on its right. Tenreiro et al. (2006) derived a criterion for the critical step height $\Delta h/H_0$ above which reflection occurs, based on estimating the strength of the vorticity patch associated with the fluid pushed back over the step, that pairs with one of the dipole parts.

The observed features of monopolar and dipolar vortices approaching step-shaped bottom topography bear some similarity to those observed in studies on barotropic coastal currents flowing

across an underwater escarpment. For example, Zavala Sansón et al.'s (2005) experimental and numerical study has revealed that the exchange of fluid between shallow and deep regions gives rise to the creation of vortex structures near the step. Similar results, obtained through contour dynamics simulations, were reported by An & McDonald (2005). A remarkable feature observed in these studies of coastal currents flowing over step topography is the formation of a weak current along the step, with shallower fluid on its right (see also Carnevale et al. 1999).

**2.4.3. Vortices over variable topography.** In a recent study, Zavala Sansón (2007) experimentally and numerically investigated the evolution and viscous decay of barotropic vortices over variable topography, consisting of a bottom topography sine-shaped in one horizontal direction and uniform in the direction perpendicular to that. The vortex structures became rapidly distorted, quickly losing their coherence. The long-term evolution of the vortex flow (extending to one or two Ekman periods) shows the alignment of vorticity structures along the topography contours, with positive relative vorticity finally distributed over deep regions and anticyclonic vorticity concentrated over shallow regions in the flow domain. This is in agreement with earlier findings of Bretherton & Haidvogel (1976), who studied numerically the adjustment of an initially random vorticity distribution over random topography. The behavior of geophysical vortices in local regions of isolated bottom topography (such as seamounts, islands, and mountains) has also been investigated both numerically and experimentally. For example, observations of Meddies (subsurface lens-shaped eddies originating from the Mediterranean outflow) colliding with seamounts in the North Atlantic Ocean and North Brazil current rings colliding with the islands of Barbados and the Lesser Antilles have triggered a number of studies (e.g., see Fratantoni & Richardson 2006; Herbette et al. 2005; Simmons & Nof 2000, 2002; Wang & Dewar 2003). This problem of a vortex near an isolated topographic feature (mountain) is also relevant in a meteorological context (see Schwierz & Davies 2003).

## 3. VORTICES IN SHALLOW FLUID LAYERS

Under the assumption that shallowness implies quasi-two-dimensional motion, laboratory experiments have been performed in nonrotating shallow layers of fluid in an attempt to model certain geophysical vortex-flow problems. In this section, we briefly review some of these experiments, including models for tidal flushing of an estuary by dipole formation, shallow-layer dipoles over a sloping bottom, and the dynamics of monopolar and dipolar vortices in a shallow fluid layer with a flat horizontal bottom.

### 3.1. Tidal Flushing by Dipole Formation

Tidal flows past a sharp headland may lead to the formation of vortical structures. Apart from forming a hazard to mariners, these vortices can have major effects on the mixing and dispersion of passive tracers and on sedimentation. Tidal flows through a narrow channel between a basin (estuary) and the open sea may give rise to sets of counter-rotating vortices. When these are sufficiently long lived, they may form a coherent dipole structure that can self-propagate away from the channel and hence promote the exchange of water and material properties between estuary and sea (e.g., see Brown et al. 2000, Fujiwara et al. 1994). The propagation of dipoles in an oscillating tidal flow has been studied experimentally by Kashiwai (1984), who found that the tidal dipoles could propagate away from the channel if the dimensionless quantity $W/UT$ (where $W$ is the channel width, $U$ is the maximum velocity in the channel, and $T$ is the tidal period) is smaller than some critical value. Wells & van Heijst (2003) developed a somewhat

more refined model. They estimated that the vorticity in the dipole formed during the outflow stage from the vorticity present in the injection channel. Under the simplifying assumption of a point vortex dipole, it was possible to describe the dipole's motion during the inflow stage, which was modeled as a potential flow due to a line sink of width $W$. The dipole could escape by outswimming the sink flow toward the channel mouth (i.e., when the quantity $W/UT$ is less than a certain value). Wells & van Heijst (2003) distinguished between two different tidal oscillations: a square wave with the channel velocity being $+U$ and $-U$ during the outflow and inflow stages, respectively, and a sinusoidal wave with $U(t) = U_0 \sin(2\pi t/T)$. For both cases, they determined the critical $W/UT$ values for dipole escape. For $W/UT$ values larger than these critical values, the dipolar structure is sucked back into the channel, leading to a rather limited exchange between the fluid compartments on either side. This is clearly visible in the dye visualization (**Figure 5*b***) obtained from the experimental setup shown in **Figure 5*a***. Apparently, the different blobs of dye undergo repeated stretching and folding in this time-dependent, quasi-two-dimensional flow, hence revealing chaotic advection. The bounded structure of the tracers is similar to Brown et al.'s (2000, their figure 7) related numerical simulation of tidal flushing of fish larvae through a narrow inlet. Vennell & Beatson (2006) report other simulations of exchange by dipole formation in a narrow tidal channel between two basins. Numerical simulations of tidal flows through constricted channels for realistic tidal situations were performed by Hench & Luettich (2003) and Zhao et al. (2006).



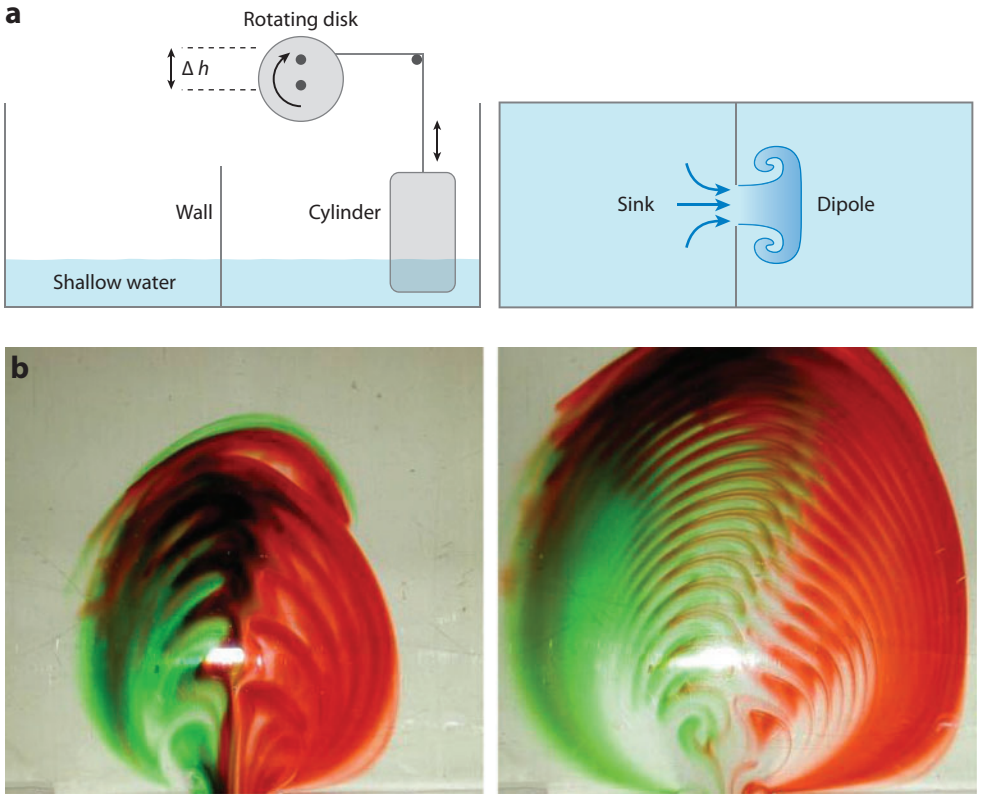


**Figure 5**

(*a*) Sketch of the laboratory setup of the tidal exchange experiments. (*b*) Visualizations of the dye dispersal in a sinusoidal-wave experiment with $W/UT > 0.13$. Green and red dyes were initially placed on one side of the opening in the separating wall. The recordings were made after 6 (*left panel*) and 25 (*right panel*) tidal periods. Figure taken from Wells & van Heijst 2003.

### 3.2. Shelving Beaches

As pointed out by Peregrine (1998) and Bühler & Jacobson (2001), a localized wave train approaching a sloping beach can generate strong mean flow vorticity at its flanks, giving rise to a dipolar vorticity structure. The motion of this vortex couple results from three different effects: its self-advection, the effect of the shoreline (domain boundary), and the self-advection due to the bottom topography. Under the assumption of two-dimensional flow, we can calculate the vortex motion mathematically by solving a rather complicated potential-vorticity inversion problem (see Richardson 2000). However, we can also obtain important insight into the dynamical behavior by adopting some simple approximations. For example, the dipole approaching the shoreline can be represented by two point vortices of strengths $\pm\gamma$ with two mirror point vortices of strengths $\mp\gamma$ to model the presence of the domain boundary. According to this simple model (see also Lamb 1932), the vortices in the pair separate when approaching the shoreline, continuing in opposite directions parallel to the coastline. In addition, the sloping bottom induces a curvature of the vortex lines in each vortex, resulting in an additional self-advection. This effect is modeled by considering the curved vortex tube as part of a large, virtual ring with radius $R$ being the distance of the vortex tube to the shoreline. As pointed out by Bühler & Jacobson (2001), the combined effect of topography and self-advection is to reduce the separation distance when the couple moves into deeper water, whereas the separation distance increases when the couple moves up the slope. Centurioni (2002) performed laboratory experiments on vortex dipoles moving toward a uniformly sloping beach, with the dipole produced by moving a plate toward the beach. The experimental results show that the dipole couple behaves as theoretically predicted, and the vortex-ring model provides accurate predictions for the along-shore propagation speed, in particular for larger values of the Reynolds number.

### 3.3. Shallow Layers with Uniform Depth

Researchers have studied the behavior of monopolar and dipolar vortices in a shallow-layer fluid with a flat horizontal bottom experimentally, either motivated by their geophysical appearance (e.g., see Jirka & Uijttewaal 2004, Lin et al. 2003, Sous et al. 2004) or as a means to study aspects of quasi-two-dimensional turbulence (e.g., see Paret & Tabeling 1997, Tabeling et al. 1991).

In many environmental flow situations, such as in rivers and estuaries, density stratification and planetary rotation are not significant, but the shallowness of the flow domain tends to suppress any vertical motions. Moreover, the no-slip bottom implies vertical gradients in the horizontal flow field, which adds to the high dissipation of turbulent flows in a shallow layer. Uijttewaal & Jirka (2003) have performed laboratory experiments on grid-generated turbulence in a shallow fluid layer, and they observed features of two-dimensional turbulence, such as growth of the characteristic length scales of the flow structures and vortex merging. To examine the dynamical behavior of elementary vortical structures in such shallow turbulent flows, Lin et al. (2003) and Sous et al. (2004, 2005) have carried out experiments on turbulent dipolar vortices generated by an impulsive horizontal jet. Depending on the forcing strength and the layer depth $H$, this forcing may result in a laminar dipolar structure that travels away from the injection region. A remarkable feature experimentally observed for larger Reynolds numbers is the presence of a band of significant vertical motion in front of the translating dipole, referred to as frontal circulation. Akkermans et al. (2008a,b) recently investigated the structure of (laminar) vortex dipoles in a shallow fluid layer experimentally by using electromagnetic forcing similar to that applied in earlier experiments (Afanasyev & Wells 2005, Boffetta et al. 2005, Paret & Tabeling 1997, Shats et al. 2005, Tabeling et al. 1991). In these experiments, the working fluid was a salt solution, in which two parallel electrode plates were positioned on opposite sides of the tank, and one or more disk-shaped

magnets could be placed underneath the thin bottom plate. The interaction of the electric current through the fluid and the magnetic field of each magnet resulted in a local Lorentz force, by which the fluid was set in motion. Akkermans et al. (2008a) used a single magnet, generating a dipolar vortex by a pulsed forcing (by briefly switching on the electric current). In contrast to Sous et al.'s (2004, 2005) experiment, the dipolar structure was now laminar, characterized by a Reynolds number of typically $Re_{dipole} = UD/\nu \simeq 1400$, where $U$ is the translation speed and $D$ is the dipole diameter. Akkermans et al. (2008a) used stereoscopic particle image velocimetry to measure the flow velocities in several horizontal cross sections of the dipolar structure (the fluid depth was varied between 6 and 11 mm, whereas the dipole diameter $D$ was typically 40 mm). **Figure 6** illustrates the flow evolution during and after the forcing. At the end of the forcing



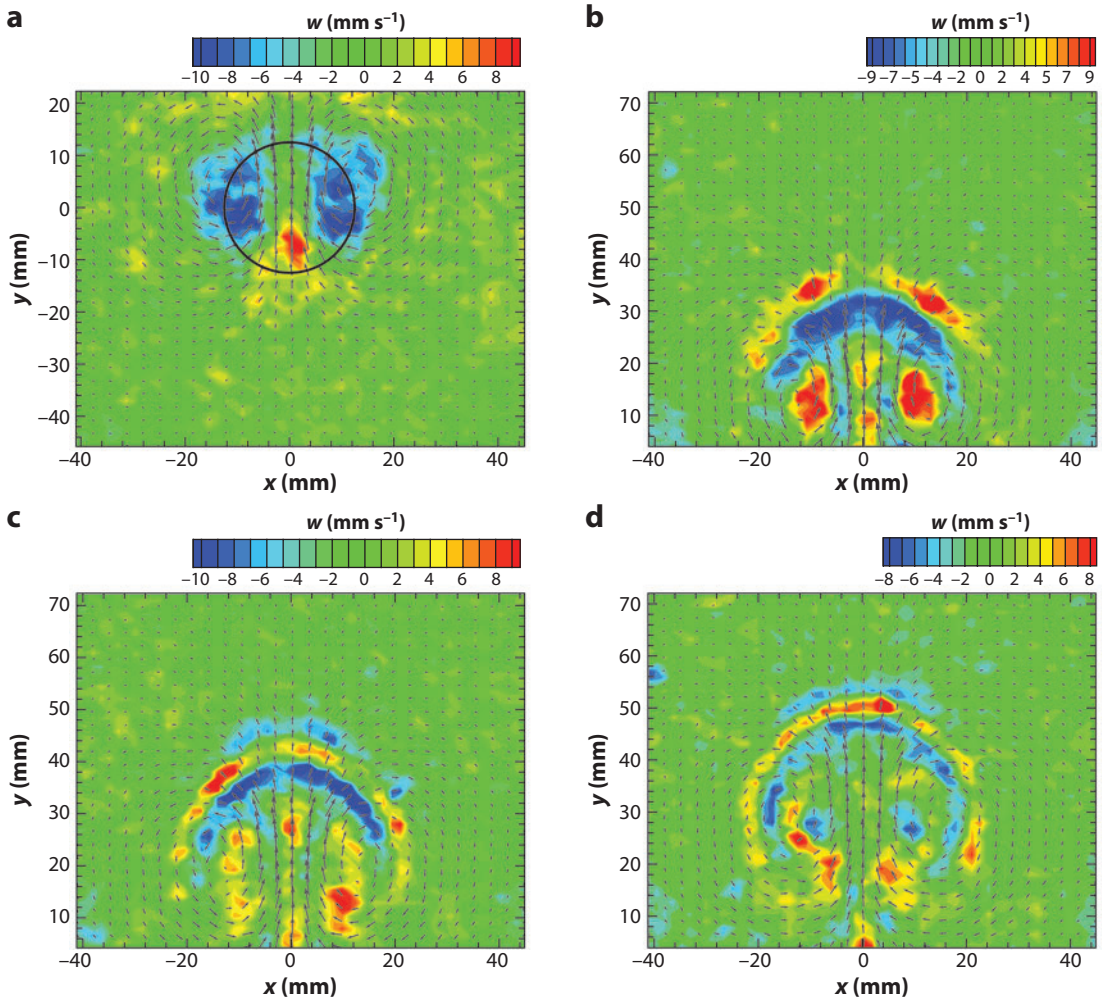


**Figure 6**

Sequence of snapshots of the velocity field measured in a horizontal cross section at a height of 5 mm in a shallow fluid layer with a depth of $H = 9.3$ mm. Vectors represent horizontal velocity components, and the colors indicate the vertical velocity magnitude. The circle denotes the position of the magnet. The snapshots were taken at $t =$ (*a*) 0.96 s, (*b*) 1.50 s, (*c*) 2.00 s, and (*d*) 2.60 s. The electromagnetic forcing was stopped at $t = 1.00$ s. Figure taken from Akkermans et al. 2008a.

(see **Figure 6*a***), one clearly observes a dipolar structure in the horizontal flow field. Somewhat surprisingly, this flow exhibits significant three-dimensional features, as evident from the patches of downward flow in the vortex cores, and an upwelling region at the rear. The downward motion in the cores results from an axial pressure gradient: Although the swirling flow in each dipole part is in good approximation in cyclostrophic balance (see Equation 10), the larger swirl velocities close to the bottom, at which the forcing is strongest, imply a lower pressure than that at the free surface.

After the forcing has been switched off, the flow shows a remarkable evolution (see **Figure 6*b*–*d***), initially with upward motion in the dipole cores and a clearly recognizable band of positive and negative vertical velocities in front of the translating dipole. This latter observation corresponds to the frontal circulation also found by Sous et al. (2004, 2005). The sign change in the vertical velocities in the dipole cores has an inertial nature: Once the forcing is switched off, the stronger swirl near the bottom is no longer maintained, and the downward flow still present after approximately $t = 1$ s (when the forcing is stopped) implies radial spreading and hence a decreasing swirl near the bottom. As a result, the pressure rises near the bottom so that the downward flow decelerates and even results in upward motion, as visible at approximately $t = 1.5$ s. This process of sign changes is repeated, and Akkermans et al. (2008a) observed typically two to three oscillations in their experiments. Finite-element numerical simulations of the shallow-layer flow subjected to this particular electromagnetic forcing agreed in even great detail with the measured flow evolution. Similar behavior was found in two-layer stratified fluid configurations, even when the bottom was taken stress-free (in the simulations). To rule out effects of the three-dimensionality of the Lorentz forces bringing the fluid in motion, Akkermans et al. (2008a) also performed numerical flow simulations with the flow initialized in the form of a Lamb-Chaplygin dipole with a Poiseuille profile in the vertical direction (see Section 2.2). The subsequent flow evolution showed the same features as in the experiments: complicated vertical motions both inside the dipole and in front of it. Apparently, such flows cannot be considered quasi–two dimensional (i.e., planar with a Poiseuille-like structure in the vertical direction).

## 4. CONCLUDING REMARKS

In this review we address some aspects of the laboratory modeling of geophysical vortices. We limit ourselves to barotropic vortices in a rotating fluid and to vortices in nonrotating shallow fluid layers. The effects of density (stratification)—although important in certain situations—are not considered as they deserve their own review article.

## DISCLOSURE STATEMENT

The authors are not aware of any biases that might be perceived as affecting the objectivity of this review.

## ACKNOWLEDGEMENTS

The authors are thankful to numerous people with whom they collaborated on the topics discussed in this article and with whom they have had enjoyable and fruitful discussions. In particular, we mention Oscar Velasco Fuentes, Luis Zavala Sansón, Mathew Wells, Rinie Akkermans, and Leon Kamp, whose work is discussed extensively here.

G.J.F.v.H. gratefully acknowledges Stuart Dalziel (DAMTP, Cambridge) for his hospitality and for providing a pleasant working environment during a few working visits. Financial support

from the research program "Two-Dimensional Turbulence" of the Foundation of Fundamental Research on Matter (FOM, The Netherlands) is also gratefully acknowledged.

## LITERATURE CITED

Adem J. 1956. A series solution for the barotropic vorticity equation and its application in the study of atmospheric vortices. *Tellus* 8:364–72

Afanasyev YD. 2002. Experiments on instability of columnar vortex pairs in rotating fluid. *Geophys. Astrophys. Fluid Dyn.* 96:31–48

Afanasyev YD, Peltier WR. 1998. Three-dimensional instability of anticyclonic swirling flow in rotating fluid: laboratory experiments and related theoretical predictions. *Phys. Fluids* 10:3194–202

Afanasyev YD, Wells J. 2005. Quasi-two-dimensional turbulence on the polar β-plane: laboratory experiments. *Geophys. Astrophys. Fluid Dyn.* 99:1–17

Akkermans RAD, Cieslik AR, Kamp LPJ, Trieling RR, Clercx HJH, van Heijst GJF. 2008a. The three-dimensional structure of an electromagnetically generated dipolar vortex in a shallow fluid layer. *Phys. Fluids* 20:116601

Akkermans RAD, Kamp LPJ, Clercx HJH, van Heijst GJF. 2008b. Intrinsic three-dimensionality in electromagnetically driven shallow flows. *Europhys. Lett.* 83:24001

An BW, McDonald NR. 2005. Coastal currents and eddies and their interaction with topography. *Dyn. Atmos. Oceans* 40:237–53

Beckers M, van Heijst GJF. 1998. The observation of a triangular vortex in a rotating fluid. *Fluid Dyn. Res.* 22:265–79

Billant P, Gallaire F. 2005. Generalized Rayleigh criterion for nonaxisymmetric centrifugal instabilities. *J. Fluid Mech.* 542:365–79

Boffetta G, Cenedese A, Espa S. 2005. Effects of friction on 2D turbulence: an experimental study of the direct cascade. *Europhys. Lett.* 71:590–96

Bretherton FB, Haidvogel DB. 1976. Two-dimensional turbulence above topography. *J. Fluid Mech.* 79:129–54

Brown CA, Jackson GA, Brooks DA. 2000. Particle transport through a narrow tidal inlet due to tidal forcing and implications for larval transport. *J. Geophys. Res.* 105:24141–56

Bühler O, Jacobson TE. 2001. Wave-driven currents and vortex dynamics on barred beaches. *J. Fluid Mech.* 449:313–39

Carnevale GF, Briscolini M, Kloosterziel RC, Vallis GK. 1997. Three-dimensionally perturbed vortex tubes in a rotating flow. *J. Fluid Mech.* 341:127–63

Carnevale GF, Kloosterziel RC. 1994a. Emergence and evolution of trianguler vortices. *J. Fluid Mech.* 259:305–31

Carnevale GF, Kloosterziel RC. 1994b. Lobe shedding from propagating vortices. *Phys. D* 76:147–67

Carnevale GF, Kloosterziel RC, van Heijst GJF. 1991. Propagation of barotropic vortices over topography in a rotating tank. *J. Fluid Mech.* 233:119–39

Carnevale GF, Shepherd TG. 1990. On the interpretation of Andrew's theorem. *Geophys. Astrophys. Fluid Dyn.* 51:1–17

Carnevale GF, Smith SGL, Crisciani F, Purini R, Serraval R. 1999. Bifurcation of a coastal current at an escarpment. *J. Phys. Oceanogr.* 29:969–85

Centurioni LR. 2002. Dynamics of vortices on a uniformly shelving beach. *J. Fluid Mech.* 472:211–28

de Ruijter WPM, van Aken HM, Beier EJ, Lutjeharms JRE, Matano RP, Schouten MW. 2004. Eddies and dipoles around South Madagascar: formation, pathways and large-scale impact. *Deep-Sea Res. I* 51:383–400

Drazin PG, Reid WH. 1981. *Hydrodynamic Stability*. New York: Cambridge Univ. Press

Dunn DC, McDonald NR, Johnson ER. 2001. The motion of a singular vortex near an escarpment. *J. Fluid Mech.* 448:335–65

Flierl GR. 1987. Isolated eddy models in geophysics. *Annu. Rev. Fluid Mech.* 19:493–530

Flierl GR, Stern ME, Whitehead JA. 1983. The physical significance of modons: laboratory experiments and general integral constraints. *Dyn. Atmos. Oceans* 7:233–63

Flór JB, Eames I. 2002. Dynamics of monopolar vortices on a topographic β-plane. *J. Fluid Mech.* 456:353–76

Fratantoni DM, Richardson PL. 2006. The evolution and demise of North Brazil Current rings. *J. Phys. Oceanogr.* 36:1241–64

Fujiwara T, Nakata H, Nakatsuji K. 1994. Tidal-jet and vortex-pair driving of the residual circulation in a tidal estuary. *Cont. Shelf Res.* 14:1025–38

Gallaire F, Chomaz JM. 2003. Three-dimensional instability of isolated vortices. *Phys. Fluids* 15:2113–26

Hench JL, Luettich RA. 2003. Transient tidal circulation and momentum balances at a shallow inlet. *J. Phys. Oceanogr.* 33:913–32

Herbette S, Morel Y, Arhan M. 2005. Erosion of a surface vortex by a seamount on a β-plane. *J. Phys. Oceanogr.* 35:2012–30

Hobson DD. 1992. A study of modon collisions using a point vortex model. *Geophys. Astrophys. Fluid Dyn.* 65:93–104

Jirka GH, Uijttewaal WSJ, eds. 2004. *Shallow Flows*. Rotterdam: Balkema

Kashiwai M. 1984. Tidal residual circulation produced by a tidal vortex. Part 1: life history of a tidal vortex. *J. Oceanogr. Soc. Jpn.* 40:279–94

Khvoles R, Berson D, Kizner Z. 2005. The structure and evolution of barotropic elliptical modons. *J. Fluid Mech.* 530:1–30

Kizner Z, Berson D, Khvoles R. 2003. Noncircular baroclinic β-plane modons: constructing stationary solutions. *J. Fluid Mech.* 489:199–228

Kloosterziel RC, Carnevale GF. 1999. On the evolution and saturation of instabilities of two-dimensional circular vortices. *J. Fluid Mech.* 388:217–57

Kloosterziel RC, Carnevale GF, Philippe D. 1993. Propagation of barotropic dipoles over topography in a rotating tank. *Dyn. Atmos. Oceans* 19:65–100

Kloosterziel RC, van Heijst GJF. 1991. An experimental study of unstable barotropic vortices in a rotating fluid. *J. Fluid Mech.* 223:1–24

Kloosterziel RC, van Heijst GJF. 1992. The evolution of stable barotropic vortices in a rotating free-surface fluid. *J. Fluid Mech.* 239:607–29

Kono J, Yamagata T. 1977. The behaviour of a vortex pair on the β-plane. *Proc. Oceanogr. Soc. Jpn.* 36:83–84 (In Japanese)

Lamb H. 1932. *Hydrodynamics*. Cambridge, UK: Cambridge Univ. Press. 6th ed.

Lin JC, Ozgoren M, Rockwell D. 2003. Space-time development of the onset of a shallow-water vortex. *J. Fluid Mech.* 485:33–66

Llewellyn Smith SG. 1997. The motion of a nonisolated vortex on the β-plane. *J. Fluid Mech.* 346:149–79

Maas LRM. 1993. Nonlinear and free-surface effects on the spin-down of barotropic axisymmetric vortices. *J. Fluid Mech.* 246:117–41

McDonald NR. 1998. The decay of cyclonic eddies by Rossby wave radiation. *J. Fluid Mech.* 361:237–52

McWilliams JC, Zabusky NJ. 1982. Interaction of isolated vortices. I. Modons colliding with modons. *Geophys. Astrophys. Fluid Dyn.* 19:207–27

Meleshko VV, van Heijst GJF. 1994. On Chaplygin's investigations of two-dimensional vortex structures in an inviscid fluid. *J. Fluid Mech.* 272:157–82

Orlandi P, Carnevale GF. 1999. Evolution of isolated vortices in a rotating fluid of finite depth. *J. Fluid Mech.* 381:239–69

Paret J, Tabeling P. 1997. Experimental observation of the two-dimensional inverse energy cascade. *Phys. Rev. Lett.* 79:4162–65

Pedlosky J. 1987. *Geophysical Fluid Dynamics*. New York: Springer

Peregrine DH. 1998. Surf zone currents. *Theoret. Comput. Fluid Dyn.* 10:295–309

Reznik GM, Grimshaw RH, Benilov ES. 2000. On the long-term evolution of an intense localized divergent vortex on the β-plane. *J. Fluid Mech.* 422:249–80

Richardson G. 2000. Vortex motion in shallow water with varying bottom topography and zero Froude number. *J. Fluid Mech.* 411:351–74

Rossby CG. 1948. On displacements and intensity changes of atmospheric vortices. *J. Mar. Res.* 7:175–87

Schwierz CB, Davies HC. 2003. Evolution of a synoptic-scale vortex advecting toward a high mountain. *Tellus* 55:158–72

Shats MG, Xia H, Punzmann H. 2005. Spectral condensation of turbulence in plasmas and fluids and its role in low-to-high phase transitions in toroidal plasma. *Phys. Rev. E* 71:046409
Simmons HL, Nof D. 2000. Islands as eddy splitters. *J. Mar. Res.* 58:919–56
Simmons HL, Nof D. 2002. The squeezing of eddies through gaps. *J. Phys. Oceanogr.* 32:314–35
Sipp D, Jacquin L. 2000. Three-dimensional centrifugal-type instabilities of two-dimensional flows in rotating systems. *Phys. Fluids* 12:1740–48
Sous D, Bonneton N, Sommeria J. 2004. Turbulent vortex dipoles in a shallow water layer. *Phys. Fluids* 16:2886–98
Sous D, Bonneton N, Sommeria J. 2005. Transition from deep to shallow water layer: formation of vortex dipoles. *Eur. J. Mech. B* 24:19–32
Sutyrin GG, Hesthaven JS, Lynov JP, Rasmussen JJ. 1994. Dynamical properties of vortical structures on the β-plane. *J. Fluid Mech.* 268:103–31
Tabeling P, Burkhart S, Cardoso O, Willaime H. 1991. Experimental study of freely decaying two-dimensional turbulence. *Phys. Rev. Lett.* 67:3772–75
Tenreiro M, Zavala Sansón L, van Heijst GJF. 2006. Interaction of dipolar vortices with a step-like topography. *Phys. Fluids* 18:056603
Trieling RR, Linssen AH, van Heijst GJF. 1998. Monopolar vortices in an irrotational annular shear flow. *J. Fluid Mech.* 360:273–94
Uijttewaal WSJ, Jirka GH. 2003. Grid turbulence in shallow flows. *J. Fluid Mech.* 489:325–44
van Geffen JHGM, Davies PA. 1999. Interaction of a monopolar vortex with a topographic ridge. *Geophys. Astrophys. Fluid Dyn.* 90:1–41
van Geffen JHGM, Davies PA. 2000. A monopolar vortex encounters a north-south ridge or trough. *Fluid Dyn. Res.* 26:157–79
van Heijst GJF. 1994. Topography effects on vortices in a rotating fluid. *Meccanica* 29:431–51
van Heijst GJF, Kloosterziel RC. 1989. Tripolar vortices in a rotating fluid. *Nature* 338:369–71
Velasco Fuentes OU, van Heijst GJF. 1994. Experimental study of dipolar vortices on a topographic β-plane. *J. Fluid Mech.* 259:79–106
Velasco Fuentes OU, van Heijst GJF. 1995. Collision of dipolar vortices on a β-plane. *Phys. Fluids* 7:2735–50
Velasco Fuentes OU, van Heijst GJF, van Lipzig NPM. 1996. Unsteady behaviour of a topography-modulated tripole. *J. Fluid Mech.* 307:11–41
Vennell R, Beatson R. 2006. Moving vessel acoustic Doppler current profiler measurements of tidal stream function using radial basis functions. *J. Geophys. Res.* 111:C09002
Voropayev SI, Eachern GB, Boyer DL, Fernando HJS. 1999. Experiment on the self-propagating quasi-monopolar vortex. *J. Phys. Oceanogr.* 29:2741–51
Wang G, Dewar WK. 2003. Meddy-seamount interactions: implications for the Mediterranean Salt Tongue. *J. Phys. Oceanogr.* 33:2446–61
Wells MG, van Heijst GJF. 2003. A model of tidal flushing of an estuary by dipole formation. *Dyn. Atmos. Oceans* 37:223–44
Zavala Sansón L. 2002. Vortex-ridge interaction in a rotating fluid. *Dyn. Atmos. Oceans* 35:299–325
Zavala Sansón L. 2007. The long-time decay of rotating homogeneous flows over variable topography. *Dyn. Atmos. Oceans* 44:29–50
Zavala Sansón L, Serravall R, Carnevale GF, van Heijst GJF. 2005. Experiments and simulations on coastal flows in the presence of a topographic slope. *J. Phys. Oceanogr.* 35:2204–18
Zavala Sansón L, van Heijst GJF. 2000. Interaction of barotropic vortices with coastal topography: laboratory experiments and numerical simulations. *J. Phys. Oceanogr.* 30:2141–62
Zavala Sansón L, van Heijst GJF. 2002. Ekman effects in a rotating flow over bottom topography. *J. Fluid Mech.* 471:239–55
Zavala Sansón L, van Heijst GJF, Backx NA. 2001. Ekman decay of a dipolar vortex in a rotating fluid. *Phys. Fluids* 13:440–51
Zavala Sansón L, van Heijst GJF, Doorschot JJJ. 1999a. Reflection of barotropic vortices from a step-like topography. *Il Nuovo Cimento* 22:C909–30
Zavala Sansón L, van Heijst GJF, Janssen FJJ. 1999b. Experiments on barotropic vortex-wall interactions on a topographic β-plane. *J. Geophys. Res.* 104:10917–32

Zehnder JA. 1993. The influence of large-scale topography on barotropic vortex motion. *J. Atmos. Sci.* 50:2519–32

Zehnder JA, Reeder MJ. 1997. A numerical study of barotropic vortex motion near a large-scale mountain range with application to the motion of tropical cyclones approaching the Sierra Madre. *Meteorol. Atmos. Phys.* 64:1–19

Zhao L, Chen C, Cowles G. 2006. Tidal flushing and eddy shedding in Mount Hope Bay and Narragansett Bay: an application of FVCOM. *J. Geophys. Res.* 111:C10015

Annual Review of
Fluid Mechanics

Volume 41, 2009

# Contents

**Indexes**



**Errata**

An online log of corrections to *Annual Review of Fluid Mechanics* articles may be found at http://fluid.annualreviews.org/errata.shtml